

## Dispersion by wind of CO<sub>2</sub> leaking from underground storage: Comparison of analytical solution with simulation

Katherine T. Schwarz<sup>a,\*</sup>, Tad W. Patzek<sup>b,1</sup>, Dmitriy B. Silin<sup>c</sup>

<sup>a</sup> University of California, Berkeley, Department of Physics, Berkeley, CA 94720, USA

<sup>b</sup> University of California, Berkeley, Department of Civil and Environmental Engineering, Berkeley, CA 94720, USA

<sup>c</sup> Earth Sciences Division, Lawrence Berkeley National Laboratory, University of California, 1 Cyclotron Road, MS90-1116, Berkeley, CA 94720, USA

### ARTICLE INFO

#### Article history:

Received 10 June 2008

Accepted 16 February 2009

Available online 21 March 2009

#### Keywords:

CO<sub>2</sub> storage

CO<sub>2</sub> leakage

Numerical simulation

Atmospheric surface layer

Advection–diffusion equation

Analytical solution

### ABSTRACT

The concentration of CO<sub>2</sub> in air near the ground needs to be predicted to assess environmental and health risks from leaking underground storage. There is an exact solution to the advection–diffusion equation describing trace gases carried by wind when the wind profile is modeled with a power-law dependence on height. The analytical solution is compared with a numerical simulation of the coupled air–ground system with a source of CO<sub>2</sub> underground at the water table. The two methods produce similar results far from the boundaries, but the boundary conditions have a strong effect; the simulation imposes boundary conditions at the edge of a finite domain while the analytic solution imposes them at infinity. The reverse seepage from air to ground is shown in the simulation to be very small, and the large difference between time scales suggests that air and ground can be modeled separately, with gas emissions from the ground model used as inputs to the air model.

© 2009 Elsevier Ltd. All rights reserved.

### 1. Introduction

Leakage of CO<sub>2</sub> from geologic sequestration into the air above ground could present health and environmental risks. Predicting the dispersion of pollutants by wind requires modeling of turbulent transport. A full description of turbulence is beyond either theory or simulation, but approximate results can be derived from an analytical model that is relatively simple, while still accounting for the variation with height of wind speed and diffusivity.

Even in the simplified model discussed in this paper, few analytical solutions are known. Many well-established models used for regulatory purposes use Gaussian plumes, which are computationally simple, but assume that wind speed and diffusivity are uniform. As a result, the plume height and decrease of ground-level concentration are underestimated. If the wind speed and diffusivity are instead assumed to follow a power-law dependence on height, there is a more general analytical solution which is just as easy to compute and potentially more accurate. The wind profile depends strongly on the temperature gradient,

which varies during the diurnal cycle of heating and cooling, and power laws with a range of powers can be used to approximate the wind profile over the range of stable and unstable temperature gradients.

This paper compares two approaches to modeling dispersion of CO<sub>2</sub> leaking from an underground reservoir into the surface layer of the atmosphere:

- (1) using a known source distribution at the surface as a boundary condition on the advection–diffusion equation describing admixture transport (Barenblatt, 2003b); and
- (2) simulating both air and ground transport together in a finite-volume code, with a logarithmic wind velocity profile (Oldenburg and Unger, 2004).

Both approaches examined here use a simplified model that assumes homogeneous flat ground and no change of wind conditions with time. More realistic descriptions would require numerical simulation of turbulence; the approaches discussed here do not actually model turbulence, but rather specify the amount of mixing that results from it. The purpose of comparing the analytical solution with the coupled simulation is in particular to investigate

- How sensitive is the solution to the velocity profile, and to the exponent in the power law?

\* Corresponding author.

E-mail address: [kts@cal.berkeley.edu](mailto:kts@cal.berkeley.edu) (K.T. Schwarz).

<sup>1</sup> Present address: University of Texas at Austin, Department of Petroleum and Geosystems Engineering, Austin, TX 78712, USA.

- How is the simulation affected by boundary conditions imposed at the edge of a finite domain?

This paper first describes the simple model of turbulent diffusion, then compares the two approaches.

## 2. A simple theoretical picture of turbulent diffusion

Trace gases are passive additives to the air, i.e., they do not affect the already existing flow field, if they are sufficiently dilute. The concentration of a passive additive is governed by the advection–dispersion equation,

$$\partial_t c + \nabla \cdot (\bar{u}c) = -\nabla \cdot \bar{F} \quad (2.1)$$

where  $c$  is the concentration,  $\bar{u}$  is the wind velocity field, and  $\bar{F}$  is the diffusive flux due to turbulent mixing;  $c$ ,  $\bar{u}$ , and  $\bar{F}$  are functions of the space coordinates  $\vec{r}$  and time  $t$ . Emission from a source can be represented by a boundary condition or source term.

In reality all these functions experience rapid turbulent fluctuations on time scales typically from about 0.1 to  $10^3$  s, but we are only concerned with the averages. Theoretically these averages should be ensemble averages, taken over different flow realizations with the same macroscopic boundary conditions. In practice with observations of weather, ergodicity is assumed so that time averages can be used instead (Monin and Yaglom, 1971, Section 3), typically over intervals of 30 min or 1 h.

The following sections will discuss the forms of wind velocity and diffusive flux that will be used in Eq. (2.1).

### 2.1. Velocity profile in the surface layer

The earth's surface exchanges momentum, heat, and mass with the atmosphere through the planetary boundary layer, which has a thickness of the order of 0.5–1 km and responds to changes in the surface over a time scale of a few hours. The planetary boundary layer is almost always turbulent. For effects near the ground, we are concerned with the surface layer, which is defined as the layer next to the ground where there are strong vertical gradients of velocity, temperature, and concentration. The surface layer is generally said to consist of about the lowest 10% of the planetary boundary layer, but there is no precise definition. In the surface layer the flow is dominated by surface friction and temperature gradient, and the Coriolis force can be neglected.

We would like to describe the wind velocity profile and the turbulent mixing in the surface layer with a minimum of measurable parameters. Our simple theoretical model assumes:

- The ground is flat and homogeneous over an area large enough that edge effects can be ignored, and therefore the flow field does not depend on the horizontal coordinates, only on height.
- The air is incompressible ( $\nabla \cdot \bar{u} = 0$ ), a good approximation in the surface layer. Together with the first assumption, this implies that the average vertical component of wind is zero.
- In the conventional coordinate system,  $z$  is height above ground and the  $x$  axis is chosen along the direction of the average wind. The velocity along this axis is the wind profile  $u(z)$ .

#### 2.1.1. Turbulence generated by surface friction

To describe turbulent flow near a rough surface when there is no heat flux, von Kármán's "law of the wall" is widely used (Arya, 1999, Section 4.7.1):

$$\frac{u(z)}{u_*} = \frac{1}{k} \ln \frac{z}{z_0} \quad (2.2)$$

where

- $u_*$  is called the friction velocity, and is defined from the shear stress at the surface,  $\tau$ , and the air density,  $\rho$ , by  $u_* = \sqrt{\tau/\rho}$ . This shear results from the covariance of turbulent fluctuations of velocity:

$$\tau = -\rho \overline{u'w'}; \text{ so } u_* = \sqrt{-\overline{u'w'}} \quad (2.3)$$

where  $u'$  and  $w'$  are the fluctuating components of horizontal and vertical velocity. Through this covariance a net downward flux of momentum is delivered from the wind to the ground. From this definition it can be seen that  $u_*$  is of the same order of magnitude as the fluctuations of velocity.

- $k$  is von Kármán's constant, which has a value of about 0.4.
- $z_0$  is a parameter called the roughness length, which depends on the details of the surface, and can be interpreted as the size of eddies at the surface; for example,  $z_0$  is of the order of  $10^{-2}$  m over grass and 1 m over forests or cities (Panofsky and Dutton, 1984, Section 6.2). The logarithmic profile would reach  $u(z) = 0$  at  $z = z_0$  if extrapolated downward, but the profile is valid only above the so-called roughness sublayer, extending to about two to five times the height of the surface irregularities, where the flow is dynamically influenced by the irregularities.

The parameters  $u_*$  and  $z_0$  can be determined by measuring  $u(z)$  at different heights and fitting a straight line to  $u$  vs.  $\ln z$ .<sup>2</sup> The length  $z_0$  is a characteristic of the surface, so after  $z_0$  is determined at a particular site,  $u_*$  can be found in other wind conditions from a measurement of  $u(z)$  at a single height.

von Kármán's law is derived from the assumption that the velocity profile becomes independent of Reynolds number in the limit of large  $Re$ ; Barenblatt (1996, 2003a) argues that this assumption is not valid and the profile does depend on  $Re$  with the form:

$$\frac{u(z)}{u_*} = \left( \frac{\sqrt{3}}{2\alpha} + \frac{5}{2} \right) \left( \frac{u_* z}{\nu} \right)^\alpha, \quad (2.4)$$

where  $\nu$  is kinematic viscosity, and  $\alpha = 3/(2 \ln Re)$ . This equation was deduced from the assumption of incomplete similarity in the nondimensionalized height  $u_* z/\nu$  and the requirement for the velocity profile to have a well-defined limit as the viscosity vanishes; the numbers  $(\sqrt{3}/2)$ ,  $(5/2)$  and  $(3/2)$  were derived from experimental data on pipe flow at various  $Re$  up to  $35 \times 10^6$ . For flow across an infinite plane,  $Re$  is not uniquely defined, and  $\alpha$  must be determined by fitting data to the curve. Barenblatt does not consider surface roughness, which is significant for any terrain rougher than very smooth ice (Sutton, 1953, Section 3.8, 7.2; Panofsky and Dutton, 1984, Section 6.2); therefore we do not expect (2.4) to hold exactly over natural terrain, but it does suggest that wind speed should depend on height through a power law.

#### 2.1.2. Turbulence generated by heat flux

There is usually a significant temperature gradient in the surface layer. During the day, as the sun heats the ground, air near the ground is warmer and less dense than air above, so it is unstable to vertical displacements. In this case buoyant forces promote turbulence and convert gravitational potential energy to turbulent kinetic energy. At night, the temperature gradient is reversed, and turbulence is suppressed. Neutral stability is rare,

<sup>2</sup>  $\overline{u'w'}$  can be measured directly with a fast-responding, three-dimensional sonic anemometer, but this is much more expensive than just measuring the mean velocity. Alternately, surface stress can be measured directly with a drag plate, but results are often unreliable (Kaimal and Wyngaard, 1990; Kaimal and Finnigan, 1994, Section 6.3).

and is only approached when the sky is heavily overcast, so the ground is not gaining or losing energy by radiation, and in addition there is moderate or high wind so the air is well mixed in temperature.

The velocity profile in thermally stratified turbulent flows is observed to deviate from the logarithmic law. Such flows are described by the Monin–Obukhov similarity theory (Monin and Yaglom, 1971, Chapter 7), which shows that by applying dimensional analysis to the fluid equations of motion, all dependence on dimensional parameters can be reduced to one dimensionless group  $z/L$ ; the Monin–Obukhov length  $L$  is defined by

$$L \equiv -\frac{u_*^3}{k(g/T_0)(q/c_p\rho)}$$

where  $g$  is gravity,  $T_0$  is the absolute temperature at the surface,  $q$  is heat flux, and  $c_p$  is the specific heat capacity of air. It can be shown that  $\zeta \equiv z/L$  represents a ratio of buoyant generation of turbulence to mechanical shear generation. Thus, at larger heights buoyant forces become more important relative to mechanical shear.

In particular, dimensional analysis shows that the velocity gradient takes the form

$$\frac{kz}{u_*} \frac{\partial u}{\partial z} = \phi_m\left(\frac{z}{L}\right). \quad (2.5)$$

The dimensionless function  $\phi_m(\zeta)$  has to be determined empirically, and must have  $\phi_m(0) = 1$  so that (2.5) reduces to (2.2) for zero heat flux. Observed wind profiles have been fit to various formulas for  $\phi_m(\zeta)$ , such as the Businger–Dyer formula (Arya, 1999, Section 4.7.2):

$$\phi_m(\zeta) = (1 + 16|\zeta|)^{-1/4}, \quad -5 < \zeta < 0 \text{ (unstable)}$$

$$\phi_m(\zeta) = 1 + 5\zeta, \quad 0 \leq \zeta < 1 \text{ (stable)}$$

The wind profile  $u(z)$  is obtained by integrating (2.5) with the boundary condition  $u(z_0) = 0$ ; as before, the profile is only valid above the roughness sublayer.

Since a direct measurement of heat flux requires expensive instruments,<sup>3</sup> formulas have been worked out to estimate  $u_*$  and  $L$  from the mean wind speed and temperature measured at two heights (Arya, 1999, Section 4.8.1; Arya, 1988, Section 11.5.6).

### 2.1.3. Power-law profile as approximate description

If the Monin–Obukhov profile is impractical (for example if it is too complex, or if temperature or other parameters are not available), meteorologists and engineers have often resorted to a simple form for the wind profile (Panofsky and Dutton, 1984, Section 6.3; Sutton, 1953, Section 7.2),

$$\frac{u}{u_1} = \left(\frac{z}{z_1}\right)^\alpha, \quad (2.6)$$

where  $u_1$  and  $z_1$  are a reference velocity and reference height, and  $\alpha$  is found by fitting the equation to measurements of  $u$  at two or more heights. Although the form (2.6) lacked theoretical justification until the work of Barenblatt (2003a), it provides a reasonable fit to wind profiles in the surface layer over a wide range of surface roughness and stability conditions, and is frequently used in air pollution modeling (Arya, 1999, Section 4.8.3).

For neutrally stratified boundary layers, the value  $\alpha = (1/7)$  is often cited in engineering texts, and was suggested by Prandtl based on experiments on pipe flow at moderate Reynolds number (Schlichting, 1968). Observed values of  $\alpha$  in the atmosphere range

<sup>3</sup> The turbulent heat flux is  $\overline{w'T'}$ , where  $T'$  is the fluctuating component of temperature; it can be measured directly by a sonic anemometer. The heat flux can also be determined from the energy budget if the radiation input and heat flux into the soil are measured.

from nearly 0 in very unstable conditions, representing perfect mixing and a uniform velocity profile, to nearly 1 in very stable conditions, approaching the Couette linear profile of laminar motion over a plane surface. The value of  $\alpha$  also depends on surface roughness: rougher surfaces have larger  $\alpha$ , corresponding to more mechanically-driven turbulence relative to buoyancy-driven turbulence.

## 2.2. Turbulent diffusion

### 2.2.1. The gradient-transport assumption

To solve (2.1) we need to know  $\vec{F}$ , the diffusive flux due to turbulent mixing, which requires further assumptions. The simplest model is an analogy to molecular diffusion: it is assumed that the flux is linearly proportional to the density gradient with some proportionality constant  $K$ :

$$\vec{F} = -K\nabla c(\vec{r}, t). \quad (2.7)$$

$K$  is called a turbulent exchange coefficient, or turbulent diffusivity. In the idealized conditions described above, with all quantities depending only on height, the flux is in the vertical direction:

$$F_z = -K \frac{\partial c}{\partial z}. \quad (2.8)$$

Similarly, the shear stress due to turbulence (defined with the opposite sign convention) is

$$\tau = \rho K_m \frac{\partial u}{\partial z}. \quad (2.9)$$

These  $K$ 's represent mixing by turbulent eddies, and are usually several orders of magnitude larger than the corresponding molecular viscosity or diffusivity.

Unlike their molecular counterparts, turbulent exchange coefficients depend on the particular flow field – rather than molecular properties – and also vary from one region to another of the same flow (Arya, 1999, Section 4.6.1). Experiments show that they depend on height above the ground: if  $K$  were spatially uniform and the wind speed were also independent of height, mass injected at a steady rate from a point source at the ground would produce a Gaussian plume, in which plume height grows with the square root of downstream distance  $x$ , and ground-level concentration decreases as  $1/x$ . However, the plume height is observed to grow as a larger power of distance, 0.75–1 instead of 0.5 (Panofsky and Dutton, 1984, Section 10.3), and the ground-level concentration also decreases faster than  $1/x$  (Sutton, 1953, p. 277). Therefore the exchange coefficient cannot be constant, but increases with height; this is because in the atmosphere, there are eddies of a wide range of sizes, and at greater heights, larger eddies contribute to mixing. The molecular diffusivity is constant because it represents mixing at only one length scale, the length scale of interaction of neighboring molecules, which is not true in turbulence.

It is sometimes assumed (e.g., Barenblatt, 2003b) that the ratio of the  $K$ 's for momentum and concentration is independent of height:

$$K(z) = (\text{constant})K_m(z). \quad (2.10)$$

This assumption implies that the mechanisms of turbulent transfer for the passive admixture are the same as for momentum. However, observations suggest that this ratio does depend slightly on  $z/L$  in unstable conditions, though not in stable conditions. The ratio at neutral stability is generally taken to be 1, although there is disagreement over this value in the literature (Kaimal and Finnigan, 1994, Section 1.3.5; Brown et al., 1993, Section 3c; Panofsky and Dutton, 1984, Section 6.9).

### 2.2.2. Implications of constant flux

Fluxes and concentration gradients are expensive to measure directly, and so various assumptions are used to estimate  $K(z)$ . The fluxes of momentum, heat, and mass are generally considered to be independent of height within the surface layer. If the assumption of constant flux is valid, then  $u_* = \sqrt{\tau/\rho}$  is independent of height. Then (2.9) can be written as

$$K_m(z) = \frac{u_*^2}{\partial_z u} \quad (2.11)$$

and using the Monin–Obukhov expression (2.5) for velocity gradient gives (Arya, 1999, Section 4.7.2; Panofsky and Dutton, 1984, Section 6.8):

$$K_m(z) = \frac{ku_*z}{\phi_m(\zeta)} \quad (2.12)$$

If instead the velocity profile follows the power law (2.6), then (2.11) becomes

$$K_m(z) = \frac{u_*^2}{\partial_z u} = \frac{u_*^2 z_1}{u_1 \alpha} \left(\frac{z}{z_1}\right)^{1-\alpha} \quad (2.13)$$

Eqs. (2.6) and (2.13) are known in meteorology as “Schmidt’s conjugate power laws.”

The turbulent diffusivity  $K$  could be derived from (2.13) combined with (2.10); however, since both these equations are only approximations,  $K$  is often modeled instead with a separate power law,

$$K(z) = K_1 \left(\frac{z}{z_1}\right)^m, \quad (2.14)$$

where  $m$  is not necessarily equal to  $1 - \alpha$ . The parameters  $K_1$  and  $m$  could be determined by fitting (2.14) to the more accurate expression (2.12), which tends to result in  $m$  slightly greater than  $1 - \alpha$  (Arya, 1999, Section 4.8.5). The power  $m$  describes how the size of the turbulent eddies increases with height: in very unstable conditions, with convective mixing,  $m$  approaches 1 and their size increases linearly with height; in very stable conditions, where turbulence is suppressed,  $m$  approaches 0 and their size becomes constant with height.

### 2.2.3. Limitations

The gradient-transport assumptions ((2.9) and (2.8)) state that the flux at a point depends only on the local gradient. This assumption fails if the eddies are large compared to the scale of curvature of the profile. If there are eddies large enough to carry air between regions of significantly different gradient, the actual flux can be non-local and even opposite the local gradient (Arya, 1999, Section 4.6.1; Panofsky and Dutton, 1984, Section 4.7.2; Pasquill and Smith, 1983, Section 3.1). Such large eddies occur most often in very unstable conditions, such as on a clear sunny day with light winds, where buoyancy-generated convection is the dominant source of turbulence. Under these conditions “looping” plumes are seen, as the large eddies move the plume as a whole back and forth, instead of the spreading or “coning” plumes predicted by gradient-transport theory (Arya, 1999, Section 6.8). Thus gradient-transport theory is most valid when mechanical shear is dominant, with slightly unstable, neutral or stable temperature profiles and strong winds.

### 2.2.4. Slender plume approximation

Turbulent diffusion in the  $x$  direction may be neglected when advection dominates dispersion in the far downwind limit, i.e.,  $x$  large compared to  $K/u$ . (Typically  $K$  is of the order of  $1-10 \text{ m}^2/\text{s}$  and  $u$  of the order of  $1-10 \text{ m/s}$ , so  $x$  should be large compared to  $1 \text{ m}$ .) It is also possible, but more cumbersome, to solve the

advection–dispersion equation (2.1) including diffusion in the  $x$  direction and then take the limit for  $x \gg K/u$ , which leads to the same result; see, for example, Sutton (1953, Section 4.6), or Huang (1979). Neglecting such diffusion is called the slender plume approximation (Arya, 1999, Section 6.3.6). With this approximation, the concentration will be zero everywhere upwind of the source.

## 3. Analytical and numerical solutions of the advection–dispersion equation

Both solutions of Eq. (2.1) discussed here make two further simplifying assumptions:

- The flow is stationary and the source remains constant in time for long enough to establish a steady-state concentration field. For the numerical simulation, this assumption was not actually necessary, but was used to provide a simple test case.
- The source is independent of the crosswind direction,  $y$ , so the concentration depends only on  $x$  and  $z$ ; that is, the problem is two-dimensional. This assumption is equivalent to considering only the crosswind integrated concentration,

$$\bar{c}_y \equiv \int_{-\infty}^{\infty} c(\vec{x}, t) dy.$$

Meteorologists sometimes use this simplification and then assume a Gaussian distribution in the lateral direction. The lateral diffusivity depends on distance from the source and atmospheric stability, and is often estimated using the empirically derived Pasquill–Gifford diagrams (Arya, 1999, Section 6.6.4; Pasquill and Smith, 1983, Section 3.2).

With these assumptions, the advection–dispersion equation (2.1) has been reduced to

$$u(z)\partial_x c(x, z) = \partial_z(K(z)\partial_z c(x, z)). \quad (3.1)$$

### 3.1. Analytical solution and interpretation

#### 3.1.1. Steady propagation from line source

Eq. (3.1) has an analytical solution when the velocity and diffusivity are given by power laws as discussed above, and the additive is emitted at a constant rate from a line source. The source is assumed to be an infinite line in the crosswind direction,  $y$ ; with a finite line source, there would be end effects where the concentration is decreased by lateral diffusion. The governing equation is thus

$$\begin{aligned} u(z)\partial_x c(x, z) &= \partial_z(K(z)\partial_z c(x, z)), \quad \text{for } x > 0 \text{ and } z > 0, \text{ with} \\ u(z) &= u_1 \left(\frac{z}{z_1}\right)^\alpha, \\ K(z) &= K_1 \left(\frac{z}{z_1}\right)^m. \end{aligned} \quad (3.2)$$

Solutions are known for boundary conditions specifying concentration at the ground, flux at the ground, or a linear combination of the two (Philip, 1959). A concentration-type boundary condition could be used, for example, to predict dispersion of pesticides volatilized from a field (Wittich and Siebers, 2002). The flux-type boundary condition will be discussed here. It is assumed that the additive is not absorbed by the ground, so the flux must vanish there:

$$K_c(z)\partial_z c \rightarrow 0 \text{ as } z \rightarrow 0. \quad (3.3)$$

There is also a boundary condition describing the source, which is located at  $x = 0, z = 0$ . Integrating (3.2) from  $z = 0$  to  $\infty$  gives

$$\begin{aligned} \partial_x \int_0^\infty u(z)c(x,z) dz &= K_c(z)\partial_z c|_0^\infty = 0, \quad \text{and so} \\ \int_0^\infty u(z)c(x,z) dz &= Q, \quad \text{a constant independent of } x. \end{aligned} \tag{3.4}$$

$Q$  is the rate of emission by the source at the origin. Since there is no absorption, in the steady state the total flux of admixture across any vertical line at  $x > 0$  is equal to the rate of emission.

3.1.2. Solution and interpretation

Eq. (3.2) with its boundary conditions (3.3) and (3.4) can be solved by the method of similarity, which applies when a function of two variables has a symmetry so that it depends only on a single, dimensionless combination of the two variables. The concentration is the product of a ground-level concentration  $c_{gl}(x)$  and a plume height function  $c_{ph}(x, z)$ :

$$c(x, z) = \begin{cases} c_{gl}(x)c_{ph}(x, z), & \text{for } x > 0 \text{ and } z > 0; \\ 0, & \text{otherwise.} \end{cases} \tag{3.5}$$

where

$$c_{gl}(x) = \frac{Q}{u_1 z_1} \frac{r}{\Gamma(\beta)} \left(\frac{x}{x_1}\right)^{-\beta},$$

$$c_{ph}(x, z) = \exp\left\{-\frac{(z/z_1)^r}{x/x_1}\right\},$$

$$r = 2 - m + \alpha, \quad \beta = \frac{1 + \alpha}{r}, \quad x_1 = \frac{u_1 z_1^2}{r^2 K_1}$$

$\Gamma(\beta)$  is the Gamma function (Abramowitz and Stegun, 1964).

Eq. (3.5) is well known in literature (Deacon, 1949; Calder, 1949; Sutton, 1953; Monin and Yaglom, 1971; Huang, 1979; Pasquill and Smith, 1983; Panofsky and Dutton, 1984; Arya, 1999). Barenblatt (2003b) explains how the solution is obtained.

Fig. 1 shows contours of  $c(x, z)$ . The first plot has  $\alpha = (1/7)$ , Prandtl's approximation for neutral stability. The second has  $\alpha = 0.3149$  chosen to fit the velocity profile in the simulation, as seen below in Fig. 4. In both cases the conjugate power law,  $m = 1 - \alpha$ , was used for the diffusivity. In the second plot, the larger  $\alpha$  and smaller  $m$  produce less mixing and less upward transport.

According to (3.5), the plume height (i.e., the height where the concentration is  $1/e$  of its value at the ground) grows as  $x^{1/r}$ , and the ground-level concentration decreases as  $x^{-\beta}$ . The concentration is inversely proportional to the wind speed  $u_1$ , as usual for advection. Some important limiting cases are:

- For uniform wind ( $\alpha = 0$ ) and uniform diffusivity ( $m = 0$ ), (3.5) reduces to a Gaussian vertical profile:

$$c(x, z) = \frac{Q/u_1}{\sqrt{\pi K_1 x/u_1}} \exp\left(-\frac{z^2}{4K_1 x/u_1}\right)$$

However, this equation is not a good fit to observed profiles in field and wind tunnel experiments (Brown et al., 1993).

- If the conjugate power laws ((2.6) and (2.13)) hold, then  $m = 1 - \alpha, r = 1 + 2\alpha$ . If  $\alpha = 1/7$  for neutral stability, this gives  $\beta = 8/9$ ; Sutton (1953, p. 281) cites observations of the propagation of smoke from a line source over level downland in neutral conditions, where the ground-level concentration was observed to decrease as  $x^{-0.9}$ , corresponding to  $\beta = 0.9$ .

This solution is the response of the system to mass injected at the line  $(x, z) = (0, 0)$ . If instead the source is spread over the

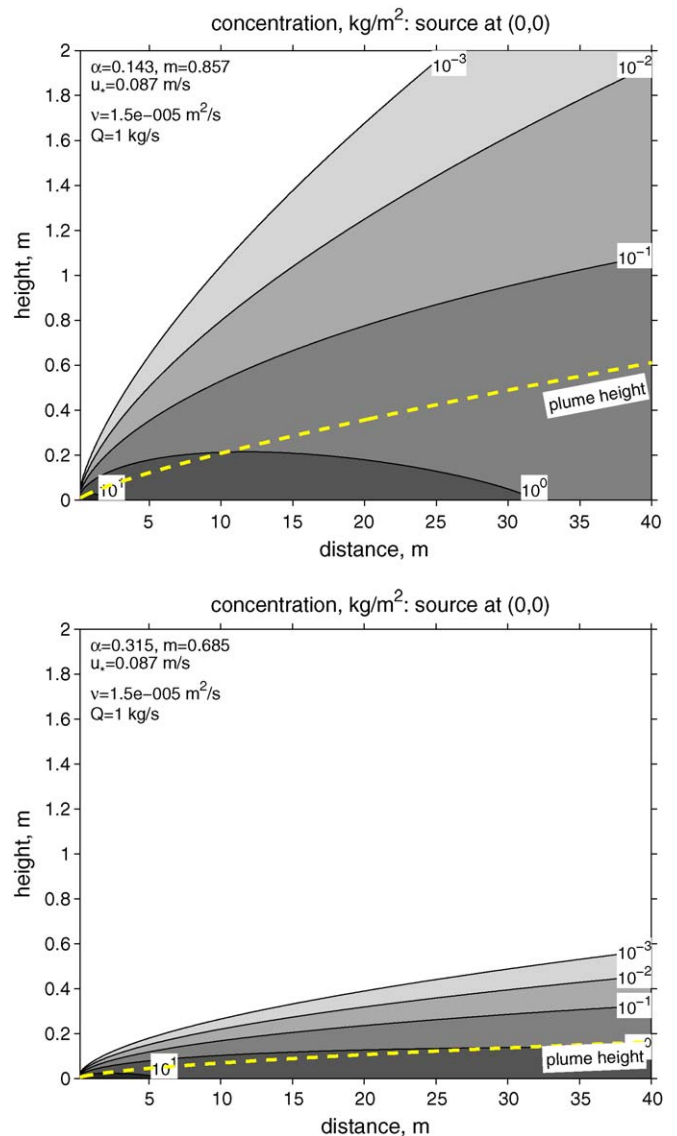


Fig. 1. Contours of plume (3.5) for two values of  $\alpha$ , representing different amounts of mixing: larger  $\alpha$  means less mixing. The dashed line shows the height where  $c(x, z)$  is  $1/e$  of its value at the ground:  $z_h = z_1(x/x_1)^{1/r}$ .

ground with a density of  $S(x)$ , the solution is the convolution

$$c_{conv}(x, z) = \int_{-\infty}^x S(x') c(x - x', z) dx' \tag{3.6}$$

where  $c(x, z)$  is the solution (3.5) for a unit source,  $Q = 1$ .

3.2. Coupled simulation of air and subsurface transport

TOUGH2 is an integral finite difference code which simulates multiphase fluid flow and heat transfer in porous media (Pruess et al., 1999; Pruess, 2004). Oldenburg and Unger (2004) used TOUGH2 to simulate the transport of  $CO_2$  emitted from a source placed at the water table at 30 m below ground, and evaluate whether it would reach hazardous concentrations above ground. The  $CO_2$  mixes with soil gas and also dissolves in groundwater, eventually seeping out of the ground.

The validity of the simulation is supported by later experiments with controlled  $CO_2$  releases, in which TOUGH2 was used to aid in the design of experiments at the Zero Emissions Research and Technology (ZERT) shallow-release facility at Montana State

University (e.g., Lewicki et al., 2007). The facility consists of a 100-meter-long horizontal well in the shallow subsurface, just below the water table, from which CO<sub>2</sub> is injected into the soil. The migration of CO<sub>2</sub> from this source was simulated for a range of injection rates in a two-dimensional domain transverse to the well, and the results were used to select an injection rate that would create a leakage signal that was challenging to detect. Although the field experiment produced a patchy seepage pattern that was not simulated by the two-dimensional model, the flux measurements agreed well with the simulation on the timing of the surface breakthrough of CO<sub>2</sub>, the overall integrated seepage flux, the rate of decrease of seepage after the end of the injection, and the extent of lateral spreading of CO<sub>2</sub> away from the well at near-steady-state conditions.

TOUGH2 is normally used for underground flow where the porosity and permeability are specified, and the flow velocity of gas and air is computed in response to boundary conditions on pressure or flow. Oldenburg and Unger modified it to include air above the ground, setting porosity to 1 in the aboveground region. The code does not actually model turbulence, but rather uses a wind profile that mimics a turbulent wind profile, and a height-

dependent diffusivity that represents the mixing due to turbulence. The wind velocity cannot be specified directly; instead, a horizontal pressure gradient was imposed, and an artificial height-dependent “permeability” was specified in the cells above ground such that Darcy’s law would yield the desired wind speed profile. The resulting horizontal wind speed was not quite independent of  $x$ , and the vertical wind speed of gas above ground was not exactly zero, perhaps due to discretization and round-off errors.

The air was modeled for heights up to 10 m; at such a small height, the departure from neutral stability is generally not significant, so the logarithmic wind profile (2.2) was used:

$$u = \frac{u_*}{k} \ln \frac{z}{z_0} \quad (3.7)$$

with  $u_*$  chosen to give a desired value of  $u$  at a reference height of  $z = 10$  m;  $k = 0.4$ ; and  $z_0 = 0.10$  m. Two wind speeds were simulated, 1 and 5 m/s.

The vertical diffusivity above ground was derived from the constant flux assumption (2.12), at neutral stability where  $\phi_m = 1$ , together with the assumption that the turbulent exchange

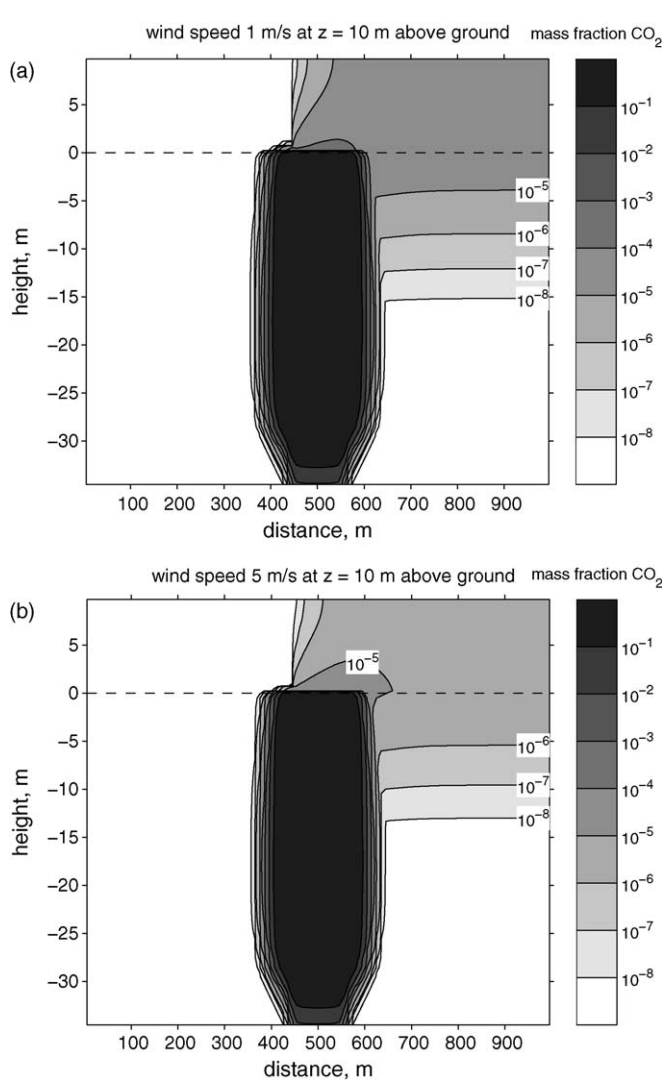


**Fig. 2.** Mass fraction CO<sub>2</sub> in gas for slow and fast wind speeds. Similar to Fig. 9ab in Oldenburg and Unger (2004); redrawn from data kindly provided by the authors. CO<sub>2</sub> is driven upward by high pressure at the source, displacing soil gas in the subsurface plume. In the second figure it can be seen that the concentration in the subsurface, where the time scale of propagation is slower, has not yet reached equilibrium with the air downwind of the source: see the 10<sup>-5</sup> contour.

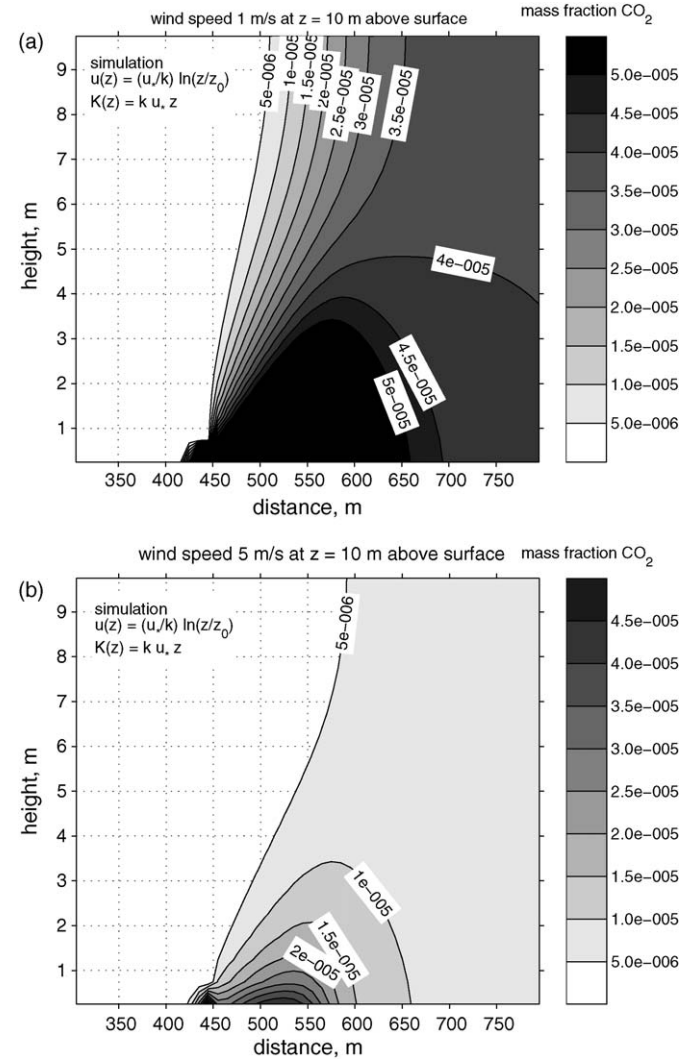


**Fig. 3.** Mass fraction CO<sub>2</sub> in gas for slow and fast wind speeds. Same data as previous figure, showing a smaller region with different contour levels. As usual for advection, the concentration is inversely proportional to wind speed (5 times smaller for the 5 times faster wind speed). Note that contour lines are perpendicular to the top surface, which is an artifact of using a closed top boundary condition. Also, the spike at  $x = 450$  m is caused by the artificial suppression of vertical dispersion upwind of the source.

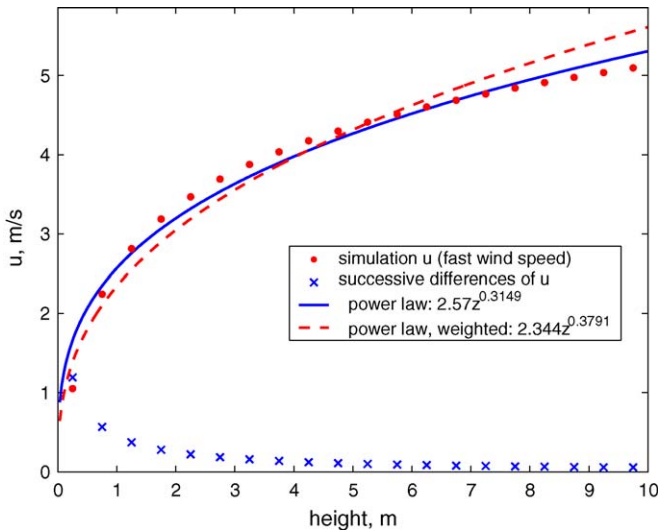


Fig. 4. Horizontal wind speed in the simulation, and power-law fits.

coefficients for momentum and mass are equal as in (2.10), giving

$$K(z) = k_u z. \tag{3.8}$$

The integral finite difference method produces numerical dispersion in the horizontal direction on the order of one-half the grid spacing multiplied by the horizontal wind velocity. This dispersion could make the plume spread upwind unrealistically; as a countermeasure, the vertical diffusivity  $K$  was set to zero upwind of the source.

Fig. 2 shows the computed mass fraction of  $\text{CO}_2$  in air at a quasi-steady state (6 months after emission begins in the simulation).

Fig. 3 shows the same data zoomed in on an area above the ground and directly above the area where  $\text{CO}_2$  was injected. These figures show selected contour lines interpolated from the grid. For clarity of comparison, the background fraction of  $\text{CO}_2$  in the atmosphere was set to zero, instead of its real value of about 380 ppmv, or about  $5.7 \times 10^{-4}$  mass fraction. Also, all other sources of  $\text{CO}_2$  besides the reservoir leak were omitted; in reality there can be a significant concentration (thousands of ppmv) in the top 1 m of soil due to respiration by soil bacteria.

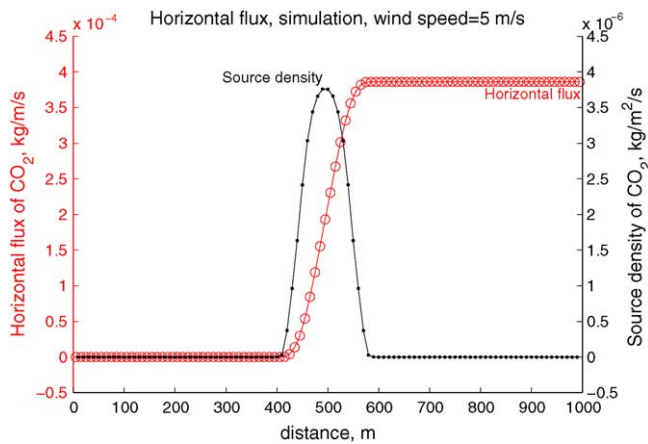


Fig. 5. Source density of  $\text{CO}_2$  from ground to air calculated from simulation result. The circles indicate total horizontal flux at gridpoints  $x_i$  calculated by  $f_i = \sum_{z_j > 0} X^{\text{CO}_2}(x_i, z_j) F_{gx}(x_i, z_j) \Delta z$ . The source density is then calculated from the successive differences,  $S_{i+0.5} = (f(x_{i+1}) - f(x_i)) / \Delta x$ . A linear interpolation of this source density is used in the convolution (3.6). The horizontal flux declines very slightly downwind of its maximum, due to reverse seepage of  $\text{CO}_2$  back into the ground; the loss is about  $10^{-5}$  of the maximum flux, too small to see on the graph.

A very small fraction of  $\text{CO}_2$  has diffused from the air back into the ground downwind of the plume, and is slowly diffusing deeper; it also dissolves in groundwater which is moving downward.

#### 4. Comparison and conclusions

##### 4.1. Comparison of two solutions

To compare this simulation with the analytic solution, the logarithmic profile was approximated by a power law. Fig. 4 shows the velocity at the grid points of the simulation, with fits to  $u = u_1 z^\alpha$  by Matlab's curve fitting tool. One fit is unweighted and the other is weighted by the difference between successive values of  $u$ ; there is no unique criterion to choose the most appropriate fit, and the unweighted fit was used for the velocity profile. The diffusivity was given by (3.8), rather than the conjugate power law (2.13), in order to match the diffusivity in the simulation.

In the simulation,  $\text{CO}_2$  passes from the ground to the air over an extended area. Therefore, it should be compared with the analytical solution using the convolution (3.6). Since the flux of

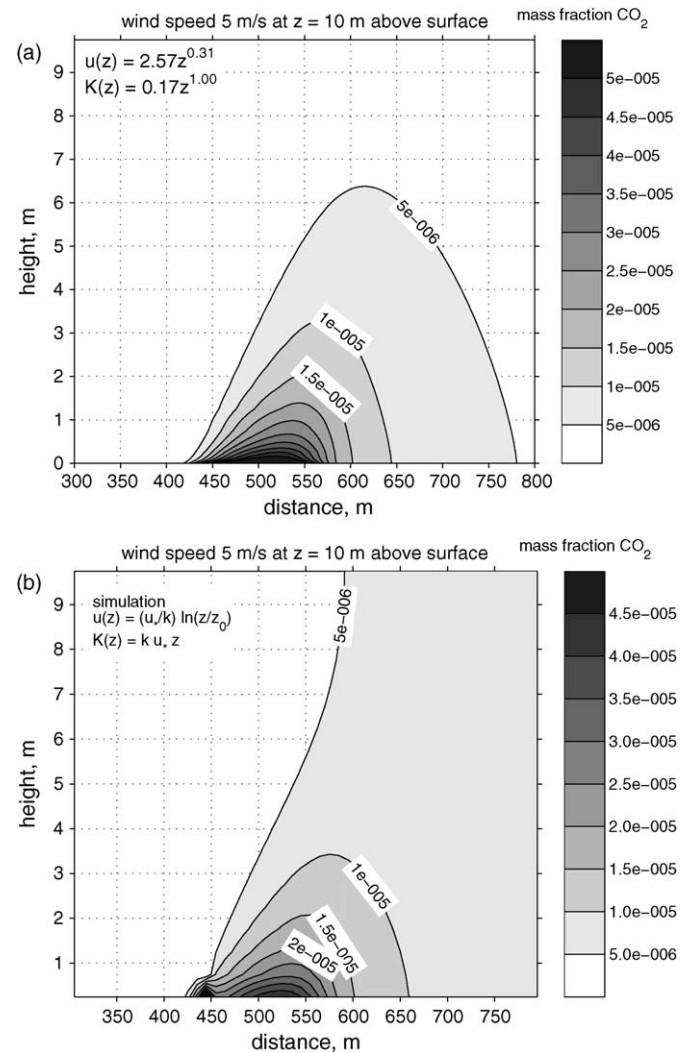


Fig. 6. (a) Convolution of line-source kernel for fast wind speeds with source distribution from Fig. 5. (b) Compare to coupled simulation (same as Fig. 3, (b)). Contours near the source and far from the side and top boundaries are similar in the two solutions. The analytical solution does not have the closed top boundary condition and the artificial barrier to upwind diffusion. The results for the slower wind speed are the same except for a factor of 5, because of the factor of  $1/u_1$  in Eq. (3.5).

CO<sub>2</sub> across the ground surface was not directly available, the source density was inferred by

$$S(x) = \frac{d}{dx} \int_0^\infty X^{\text{CO}_2}(x, z) F_{gx}(x, z) dz,$$

$X^{\text{CO}_2}$  = mass fraction CO<sub>2</sub> in gas,  $F_{gx}$  = horizontal flux of gas

which is shown in Fig. 5. The reverse seepage flux of CO<sub>2</sub> back into the ground can also be calculated, since the horizontal flux declines very slightly downwind of its maximum at about  $x = 600$  m; the loss is about  $10^{-5}$  of the maximum flux. The source density for the other data set (wind speed 1 m/s) was indistinguishable, because the seepage of CO<sub>2</sub> was driven by a high pressure at 30 m below the surface, and did not depend on the wind speed above the ground.

Fig. 6 shows the result of the convolution (3.6) and compares it with the simulation. It is qualitatively similar to the TOUGH2 plume, but does not show the artifacts of the closed top boundary condition and the suppression of upwind diffusion.

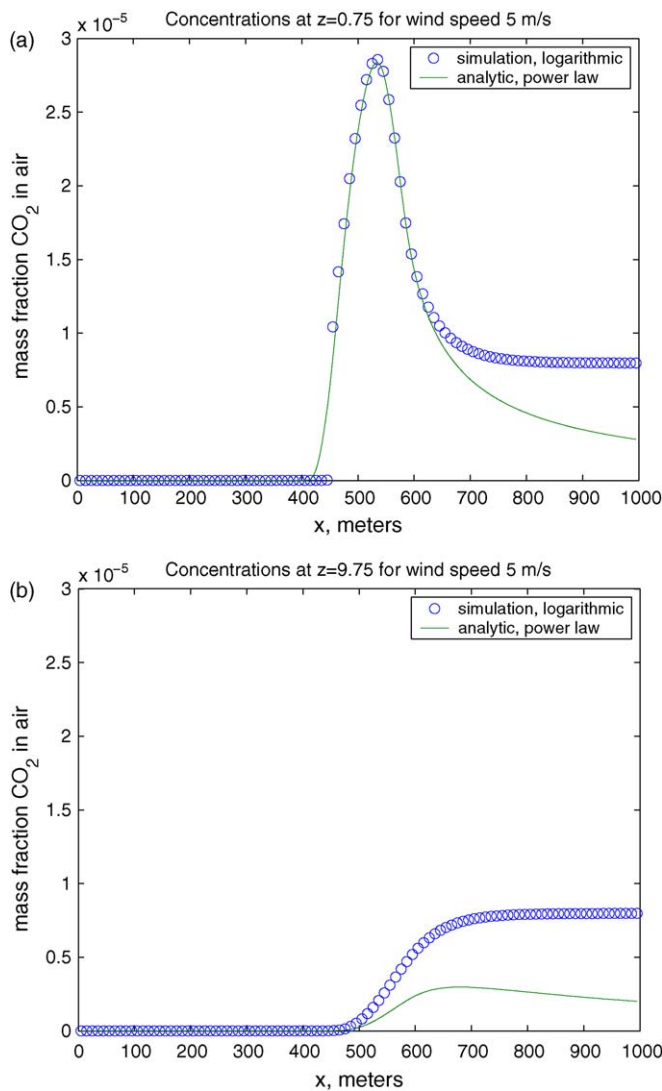


**Fig. 7.** The two solution methods compared at heights of  $z = 0.75$  and  $9.75$  m. The concentration in the simulation decays more slowly with downwind distance, probably because a zero-gradient side boundary condition was used (i.e.,  $\partial c / \partial x = 0$  at  $x = 1000$ ), which causes the concentration to reach a constant value at relatively small downwind distances, instead of decaying to zero only asymptotically as  $x \rightarrow \infty$ . Near the top, the concentration in the simulation is more than twice as large, likely because of the closed top boundary condition. Both these boundary conditions would lead to accumulating CO<sub>2</sub> in the simulation, rather than letting it escape to infinity in the vertical and horizontal.

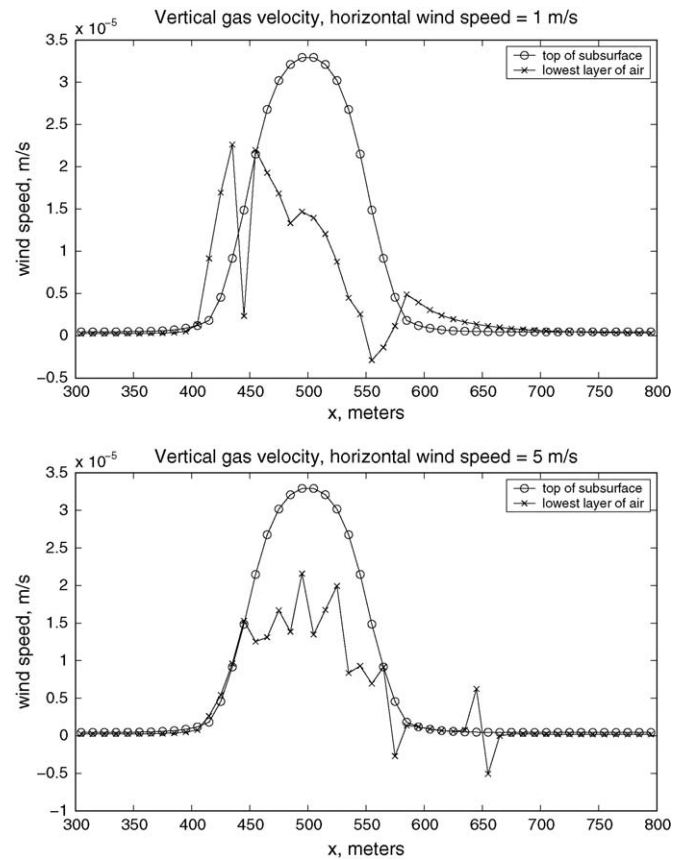


**Fig. 8.** Vertical gas velocity in the simulation at the top layer of the subsurface and the bottom layer of air.

Fig. 7 shows how the concentrations depend on downwind distance at  $z = 0.75$ , near the ground, and at  $z = 9.75$ , the top of the simulation. The results are close near the source but differ at the top and side, because different boundary conditions were imposed there.

The aboveground domain has much shorter inherent time scales than the underground domain. In the simulation, the permeability changes abruptly from 1 darcy just below the ground to  $2 \times 10^9$  darcy just above, and from horizontal gas speeds of the order of  $10^{-7}$  m/s below to 1 m/s above. It is difficult for the code to maintain accurate calculations at such a boundary. Fig. 8 illustrates how the smooth distribution of vertical gas velocities under the surface suddenly becomes irregular and noisy in the air.

#### 4.2. Conclusions

Both approaches described here are limited by the highly idealized model of turbulent diffusion: the gradient-transport model assumes that turbulent transport of momentum and mass is local, just like diffusion with a different constant of diffusivity, as described in Section 2. The velocity profiles described in Section 2 apply only to heights above any surface obstacles and large compared to  $z_0$ ; they assume flat ground with short, homogeneous vegetation. Modeling the roughness sublayer, where there can be significant turbulent transport in cities and forests, would be far more complex.

The concentrations computed from the analytic solution, using a power-law profile fit to the logarithmic velocity profile over a limited range of heights, are close to the numerical simulation result in the part of the domain far from the boundaries. Near the side and top boundaries, the two solutions are significantly

different. The simulation has no vertical flux at the top ( $z = 10$  m) and zero concentration gradient at the side ( $x = 1000$  m). The analytic solution obeys these same conditions at  $z \rightarrow \infty$  and  $x \rightarrow \infty$  respectively, instead of finite values. This result suggests that the simulation would be more realistic with a larger domain size, but then the computational cost would be greater.

The TOUGH2 coupled simulation can model barometric pumping and reverse seepage of air contaminants back into the ground when these phenomena could be significant, such as with large soil permeability. But the underground and aboveground domains operate on vastly different time and space scales, which suggests separating the domains whenever they are not strongly coupled. We expect on *physical* grounds that the air above ground is not usually coupled to the subsurface, because the capillary entry pressure for gas into the ground is high enough that the ground can be treated as a reflecting boundary. In fact, this was a good approximation in the case used for the simulation, as shown by getting the same emission rate out of the ground for both wind speeds. If the main goal is to predict concentrations in the air, the small reverse seepage (only  $10^{-5}$  as great as the total flux of  $\text{CO}_2$  into the air) could be neglected.

Each approach has advantages and disadvantages. Some advantages of the analytical solution, as opposed to the coupled simulation, are:

- It is computationally simple and needs no programming, while still allowing variation of  $K$  with height.
- It does not suffer from the closed-top boundary condition imposed by TOUGH2 (although TOUGH2 could work around this limitation by adding a very large grid block above the layer of interest to receive the upward flux). The solution is independent of where the boundaries of the domain are placed.
- It does not have the artificial horizontal dispersion which accompanies advection in the numerical solution.
- There is no minimum grid cell size. TOUGH2 cannot make the grid cell smaller than the roughness length,  $z_0$ , while using the logarithmic velocity profile.
- There are no problems of finite precision.

#### Disadvantages of the analytical solution:

- The solution is known only for power-law profiles. It is questionable how accurately a logarithmic or Monin–Obukhov profile can be approximated by a power law. In particular, the diffusivity will always grow more slowly at large heights for power laws than for the logarithmic profile.
- It cannot describe a time-dependent source profile, which could easily be handled in TOUGH2.
- It assumes homogeneous flat terrain, which is invalid for most natural areas.
- The slender plume approximation fails for wind speeds approaching zero, which is also the worst condition for building up high local concentrations of contaminants.

The most important generalization and improvement to this model is to take into account the behavior of dense gas in terrain with valleys, since that is where  $\text{CO}_2$  is most likely to collect in concentrations that are hazardous to humans. For example, [Chow et al. \(2008\)](#) modified a large-eddy simulation code to allow for dense gas transport, and found that an instantaneously released mass of  $\text{CO}_2$  could remain concentrated in a valley even under winds that quickly remove a passive admixture, and hazardous concentrations could be retained in topographic depressions of 10–50 m depth.

Still, the analytic solution is much simpler to use than a full numerical simulation, and can be useful as a simple prediction of pollutant plumes in flat terrain when the wind and diffusivity profiles are known and the problem involves only steady-state conditions. Related solutions for flat area sources can be used to predict the concentration of pesticide vapors downwind from agricultural fields ([Wittich and Siebers, 2002](#)) or the flux of greenhouse gases from surface waters.

#### Acknowledgments

We are grateful to Dr. C.M. Oldenburg of Lawrence Berkeley National Laboratory, Earth Sciences Division, for sharing his data, helping us interpret it, and carefully reviewing this paper. Dr. N.L. Miller of LBNL also reviewed the paper. The authors would also like to thank Professor G.I. Barenblatt, who read an early version of the paper and provided very useful discussions.

This work has been performed at University of California, Berkeley, and Lawrence Berkeley National Laboratory of the U.S. Department of Energy under Contract No. DE-AC02-05CH11231. Support for the first author was provided by a Sunset Fellowship from the Center for Pure and Applied Mathematics at UC Berkeley.

#### References

- Abramowitz, M., Stegun, I.A., 1964. Handbook of Mathematical Functions with Formulas, Graphs, and Mathematical Tables, 9th Dover printing 10th GPO printing edn. Dover, New York.
- Arya, S.P., 1988. Introduction to Micrometeorology. Academic Press.
- Arya, S.P., 1999. Air Pollution Meteorology and Dispersion. Oxford University Press.
- Barenblatt, G.I., 1996. Scaling, Self-similarity, and Intermediate Asymptotics. Cambridge University Press.
- Barenblatt, G.I., 2003a. Scaling. Cambridge University Press.
- Barenblatt, G.I., 2003b. Transfer of a Passive Additive in a Turbulent Boundary Layer at Very Large Reynolds Numbers. Proceedings of the National Academy of Sciences, USA 100, 1481–1483.
- Brown, M.J., Arya, S.P., Snyder, W.H., 1993. Vertical dispersion from surface and elevated releases: an investigation of a non-Gaussian plume model. Journal of Applied Meteorology 32, 490–505.
- Calder, K.L., 1949. Eddy diffusion and evaporation in flow over aerodynamically smooth and rough surfaces: a treatment based on laboratory laws of turbulent flow with special reference to conditions in the lower atmosphere. Quarterly Journal of Mechanics and Applied Mathematics 2, 153–176.
- Chow, F.K., Granvold, P.W., Oldenburg, C.M., 2008. Modeling the effects of topography and wind on atmospheric dispersion of  $\text{CO}_2$  surface leakage at geologic carbon sequestration sites. Energy Procedia, GHGT9 conference, November 16–20, 2008, Washington DC., LBNL-1420E.
- Deacon, E.L., 1949. Vertical diffusion in the lowest layers of the atmosphere. Quarterly Journal of the Royal Meteorological Society 75, 89–103.
- Huang, C.H., 1979. A theory of dispersion in turbulent shear flow. Atmospheric Environment 13, 453–463.
- Kaimal, J.C., Finnigan, J.J., 1994. Atmospheric Boundary Layer Flows: Their Structure and Measurement. Oxford University Press.
- Kaimal, J.C., Wyngaard, J.C., 1990. The Kansas and Minnesota experiments. Boundary-Layer Meteorology 50, 31–47.
- Lewicki, J.L., Oldenburg, C.M., Dobeck, L., Spangler, L., 2007. Surface  $\text{CO}_2$  leakage during two shallow subsurface  $\text{CO}_2$  releases. Geophysical Research Letters 34, L24402.
- Monin, A.S., Yaglom, A.M., 1971. Statistical Fluid Mechanics: Mechanics of Turbulence. MIT Press. English edition updated, augmented and revised by the authors.
- Oldenburg, C.M., Unger, A.J., 2004. Coupled Vadose zone and atmospheric surface-layer transport of carbon dioxide from geologic carbon sequestration sites. Vadose Zone Journal 3, 848–857.
- Panofsky, H.A., Dutton, J.A., 1984. Atmospheric Turbulence: Models and Methods for Engineering Applications. Wiley.
- Pasquill, F., Smith, F.B., 1983. Atmospheric Diffusion, 3rd edn. Ellis Horwood.
- Philip, J.R., 1959. The Theory of Local Advection. I. Journal of Meteorology 16, 535–547.
- Pruess, K., 2004. The TOUGH codes—a family of simulation tools for multiphase flow and transport processes in permeable media. Vadose Zone Journal 3, 738–746.
- Pruess, K., Oldenburg, C.M., Moridis, G.J., 1999. TOUGH2 User's Guide. Version 2. Lawrence Berkeley National Laboratory. Paper LBNL-43134. Available at <http://repositories.cdlib.org/lbnl/LBNL-43134>.
- Schlichting, H., 1968. Boundary-Layer Theory, 6th ed. McGraw-Hill.
- Sutton, O.G., 1953. Micrometeorology. McGraw-Hill.
- Wittich, K.-P., Siebers, J., 2002. Aerial short-range dispersion of volatilized pesticides from an area source. International Journal of Biometeorology 46, 126–135.